THE GEOLOGICAL SOCIETY OF AMERICA®

Constraining the early Eocene climatic optimum: A terrestrial interhemispheric comparison

Ethan G. Hyland[1,†], Nathan D. Sheldon[1], and Jennifer M. Cotton[1,2]

[1]*Department of Earth and Environmental Sciences, University of Michigan, 1100 North University Avenue, Ann Arbor, Michigan 48109, USA*

[2]*Department of Geological Sciences, California State University, Northridge, 18111 Nordhoff Street, Northridge, California 91330, USA*

ABSTRACT

The early Eocene climatic optimum was a period of major climatic and environmental change that was caused by perturbations to the global carbon cycle. Recent work from terrestrial sections in the Northern Hemisphere demonstrates that the period was characterized by different responses in the terrestrial and marine realms, suggesting that traditional causal mechanisms may not adequately explain the dynamics of the early Eocene climatic optimum. Here, we present a new high-resolution multiproxy record of terrestrial climatic and environmental conditions during the early Eocene climatic optimum from the Southern Hemisphere and compare this reconstruction to other marine and terrestrial records. Similar to Northern Hemisphere terrestrial records, there is a transient peak period of atmospheric carbon isotope enrichment as well as increased temperatures and precipitation, which indicate that terrestrial environmental responses to the early Eocene climatic optimum were broadly consistent in temperate settings worldwide. This global consistency in terrestrial records demonstrates differences in peak warming time scales and carbon isotope responses between marine and terrestrial systems, which further constrain potential causes for the early Eocene climatic optimum to multiple-system or nontraditional mechanisms and highlight the importance of paired records for understanding past climate.

INTRODUCTION

The peak of the early Eocene climatic optimum occurred from 53 to 50 Ma as the culmination of a prolonged period of global warming and climatic change (e.g., Zachos et al., 2008). It was accompanied by substantial shifts in greenhouse gas concentrations, global temperatures, and precipitation patterns, as well as floral and faunal biogeographies, and it may be one of the best available analogues for future climatic conditions in a high-CO_2 world (>500 ppm; e.g., Rohling et al., 2012). The climate impacts and ecological responses of the early Eocene climatic optimum are well described and robustly modeled for regions such as North America and the Pacific Ocean (e.g., Zachos et al., 2008; Smith et al., 2008; Thrasher and Sloan, 2009; Huber and Caballero, 2011; Hollis et al., 2012; Lunt et al., 2012), but the primary cause of the high carbon dioxide concentrations that led to the peak conditions of the early Eocene climatic optimum remains highly contentious (e.g., Kent and Muttoni, 2008; Smith et al., 2014; Turner et al., 2014). Descriptions of the cause of these changes fundamentally affect both the ways in which global carbon cycle dynamics are understood and modeled, and their potential predictive value for future climate change.

While proxy and model-based estimates of the magnitude of change in global temperature increases (~6 °C; e.g., Greenwood and Wing, 1995; Hollis et al., 2012), regional precipitation increases (up to 600 mm yr^{-1}; e.g., Shellito et al., 2003; Hyland et al., 2013), and atmospheric CO_2 concentration increases (~1000 ppm; e.g., Demicco et al., 2003; Hyland and Sheldon, 2013) are somewhat constrained for the early Eocene climatic optimum, the release time scale and source of carbon responsible for these peak conditions are unclear due to the complicated nature of terrestrial-atmospheric-oceanic interactions in the carbon cycle. Until recently, nearly all of the available early Eocene climate proxy data came from ocean sediments (e.g., Zachos et al., 2008; Hollis et al., 2012), but new terrestrial proxy data from both western North America and now central South America (Fig. 1) have shed light on discrepancies between the changes recorded in terrestrial and marine proxy materials (e.g., Krause et al., 2010; Hyland and Sheldon, 2013; Hyland et al., 2013), particularly in terms of the time scale of peak climatic changes and the direction of carbon isotope responses in the different systems.

A comparison of marine and terrestrial records is crucial for detailing the dynamics of the global climate system and for understanding the changes in the carbon cycle that led to the early Eocene climatic optimum. Here, we compile multiproxy terrestrial records from North America and present a new record from South America (Argentina) as the first interhemispheric comparison of the impacts of the early Eocene climatic optimum on regional climates and the carbon cycle on land, and we place this work within the context of established marine proxy trends during the early Eocene in an attempt to reevaluate potential causal mechanisms for the peak early Eocene climatic optimum.

METHODS

To expand and improve paleoclimatic reconstructions of the early Eocene climatic optimum in the Southern Hemisphere, we constructed a multiproxy record throughout the early Eocene for a site in the Salta Basin of northwestern Argentina (Cerro Bayo; Fig. 1). The Cerro Bayo section contains a series of fluvio-lacustrine sediments deposited in the Salta Basin (paleo–Lake Alémania) during the early Paleogene (Marquillas et al., 2005). While the Salta Basin now resides at moderate elevations in the subtropics (near 25°S), deposition originally occurred at lower elevations (<1 km; Marquillas et al., 2005) and at temperate latitudes around 38°S (±3°; van Hinsbergen et al., 2015), making the Cerro Bayo section a robust comparison point for many of the other available temperate zone terrestrial records of the early Eocene climatic optimum.

The age of this record was constrained through local biostratigraphy and magnetostratigraphic sampling of the upper Cerro Bayo sec-

†Department of Earth and Space Sciences, University of Washington, 4000 15th Avenue NE, Seattle, Washington 98195, USA; hylande@uw.edu.

GSA Bulletin; January/February 2017; v. 129; no. 1/2; p. 244–252; doi: 10.1130/B31493.1; 5 figures; Data Repository item 2016299; published online 18 October 2016.

tion in the Salta Basin (Fig. 1; Maíz Gordo Formation) to determine local normal and reversed polarity intervals and to tie the local polarity pattern to the geomagnetic polarity time scale (GPTS; Gradstein et al., 2012). Paleomagnetic sampling included block sampling of multiple lithologies (siltstone, fine sandstone), which were oriented in the field using a Brunton Field Transit compass on cleared bedding planes; specimen cores were drilled using a drill press from oriented hand samples at the University of Michigan Paleomagnetism Laboratory.

Stepwise thermal demagnetization from 100 °C to 700 °C (regular 50 °C steps to 500 °C, regular 25 °C steps thereafter) used an ASC thermal demagnetizer and a 2G cryogenic magnetometer. Analysis of 25 sampling levels (~5 m interval) yielded reliable characteristic remanent magnetization (ChRM) directions at 24 levels (Data Repository Fig. DR1; Table DR1[1]). ChRM directions from vector end-point diagrams were calculated on a minimum of 5 measurements (250–600 °C) using Virtual Paleomagnetic Directions software (Ramón and Pueyo, 2008; Fig. DR1 [see footnote 1]). Sample means were calculated for ~3 individual cores for each sample level, and samples with a mean angular deviation (MAD) >15° were rejected from further analysis (resultant MAD values for samples averaged 8.6°); all other samples were bedding and tilt corrected, and statistical models were applied to verify data quality (e.g., reversals test, Fisher means; Ramón and Pueyo, 2008).

Paleosols were identified based on field characteristics such as horizonation, pedogenic features (carbonate nodules, clay slickensides), and other surficial features (root traces, burrows), and they were classified and described in detail (e.g., Mack et al., 1993; NRCS, 2014; Fig. DR2 [see footnote 1]). Paleosols were trenched to avoid modern contamination, and samples were collected within measured local stratigraphy and analyzed for both the major-element composition of paleosol bulk samples and the carbon isotope composition of paleosol A-horizon samples. Major-element data (Table DR2 [see footnote 1]) from paleosol geochemical analyses (XRF analyses performed at ALS Chemex Laboratory) of identified B-horizons were input into weathering climofunctions, using the salinization index (SAL; Sheldon et al., 2002) and the paleosol weathering index (PWI; Gallagher and Sheldon, 2013) to reconstruct mean annual temperature (MAT; standard errors = ±4 °C and ±2 °C, respectively) and the chemical index of alteration minus potassium (CIA-K; Sheldon et al., 2002) to reconstruct mean annual precipitation (MAP; standard error = ±182 mm yr^{-1}).

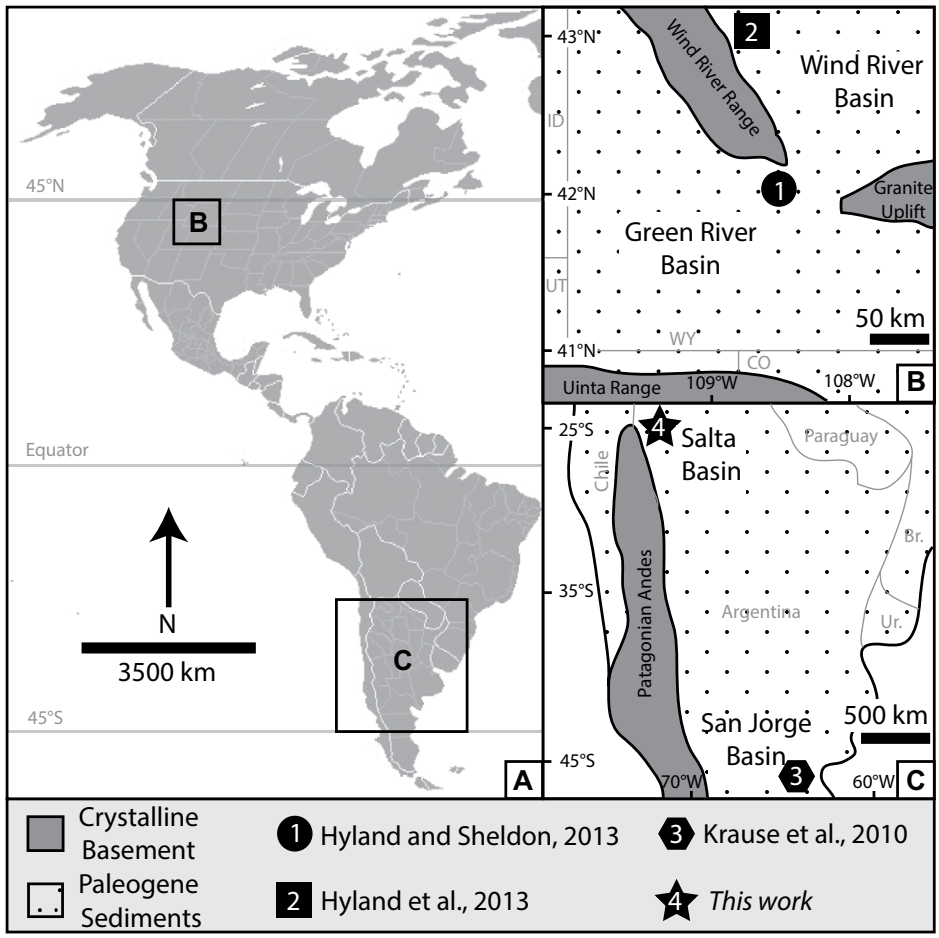

Figure 1. (A) Sites of terrestrial early Eocene climatic optimum reconstructions and detail of the (B) Northern and (C) Southern Hemisphere sites. ID—Idaho, UT—Utah, WY—Wyoming, CO—Colorado; Br—Brazil, Ur—Uruguay.

Each of these paleosol geochemical methods has been used worldwide to describe climatic and environmental change during at least the Mesozoic–present (e.g., Retallack, 2007; Hyland and Sheldon, 2013), and they have also proven robust in comparisons with independently derived terrestrial paleoclimate proxies (e.g., Sheldon et al., 2002; Retallack, 2007; Hyland et al., 2015a). In order to ensure that changing paleosol chemistry reflects changes in weathering intensity rather than changing sedimentary provenance, Ti/Al ratios were used to screen paleosol profiles, where constant values indicate stability, and variable values or a stratigraphically defined shift indicate changing provenance (Driese, 2004; Sheldon and Tabor, 2009).

Stable carbon isotope data were generated from preserved roots and dispersed soil organic carbon, which were sampled from paleosol A-horizons and cleaned of modern organics by ultrasonication in methanol. Samples were acidified with 7% HCl to remove carbonate, rinsed, and homogenized before being weighed into solvent-washed tin capsules (e.g., Cotton et al., 2012) and analyzed at the University of Michigan Stable Isotope Laboratory on a Costech ECS4010 elemental analyzer attached to a Thermo Delta V+ isotope ratio mass spectrometer. Results are presented in units per mil (‰) relative to the Vienna Peedee belemnite, and analyses used International Atomic Energy Agency (IAEA) sucrose and caffeine as internal standards to normalize measured values; analytical uncertainty for all analyses was maintained at <0.1‰ (Table DR3 [see footnote 1]). Preserved organic carbon from paleosols and fluvial sediments has been used extensively in developing carbon isotope stratigraphies of similar large continental basins during the Paleogene (e.g., Foreman et al., 2012; Abels et al., 2012; Smith

[1]GSA Data Repository item 2016299, paleomagnetic, paleosol, and isotope data, is available at http://www.geosociety.org/pubs/ft2016.htm or by request to editing@geosociety.org.

et al., 2014), and for reconstructing atmospheric carbon dioxide concentrations and carbon cycle conditions from paleosol sequences throughout the Cenozoic (e.g., Cotton et al., 2012; Hyland and Sheldon, 2013).

RESULTS

Age Model

Magnetostratigraphic samples were universally demagnetized between 500 °C and 700 °C, suggesting magnetite as the primary ChRM carrier, and resultant sample vectors define normal and reversed polarity stable components that cluster into two nearly antipodal groups with Fisher means at declination (D) = 170°, inclination (I) = 33° (a_{95} = 12.8) and D = 358°, I = –39° (a_{95} = 13.5). The two mean poles pass a reversals test, and their directions are distinct from the modern direction while fitting an expected Paleogene direction from NW Argentina (Fig. DR1 [see footnote 1]; Prezzi and Alonso, 2002). These samples define polarity zones, each of which is based on multiple stable sample levels (>3), and they are mostly well constrained (<1 m) and unambiguous zones, except for the single basal sample, which suggests a possible transitional zone (Fig. 2). Paleontological age constraints based on mammalian and palynofloral records known from the base and upper Maíz Gordo Formation (Fig. 2; Quattrocchio and Volkheimer, 2000; Gelfo et al., 2009) place this section in the Itaboraian South American Land Mammal Age (SALMA), and the revised SALMA time scales of Woodburne et al. (2014) and Clyde et al. (2014) therefore place the section in the early Eocene (ca. 54–50 Ma).

When the local polarity time scale is then compared to global results for the early Eocene (GPTS; Gradstein et al., 2012), it produces four possible absolute age correlations, as shown in Figure 2. Scenario 1 correlates to C24n.3n-C22r, with relatively constant moderate deposition rates (~40–50 m m.y.$^{-1}$). This scenario assumes that our magnetostratigraphic record does not capture short-duration (<0.15 m.y.) subchrons like C24n.2n and C23n.1r (Fig. 2), which is fairly likely due to the lower sampling resolution of this formation (cf., Hyland et al., 2015b). Relatively constant moderate deposition rates are also consistent with sedimentological observations; the formation shows little evidence for changes in lithology or depositional mode throughout (e.g., Marquillas et al., 2005), and the moderate sedimentation rate agrees with estimates from depositional constraints provided by detrital zircon and apatite fission-track uplift models of these formations in the basin and surrounding region (~25–50 m m.y.$^{-1}$; DeCelles et al., 2011).

Scenario 2 correlates to C24n.3n-C23r, with relatively constant high deposition rates (~105–175 m m.y.$^{-1}$). While constant, this scenario has unreasonably high sedimentation rates compared to both independent estimates (~3× higher than DeCelles et al., 2011) and to soil formation models, which suggest that well-developed calcic and argillic soils like those observed extensively here (>12 paleosol profiles; Fig. DR2 [see footnote 1]) require somewhat slower deposition (e.g., Retallack, 2001). Scenario 3 correlates to C23n.2n-C21r, with variable but moderate sedimentation rates (~20–75 m m.y.$^{-1}$). This scenario is unreasonable due to both the abrupt change in sedimentation rate in a part of the formation that lacks any apparent facies change (Fig. 2), and due to the higher sedimentation rate at the base of the formation, which is characterized by lacustrine deposition and paleosol formation and should therefore represent a period of relatively slower rates (e.g., Marquillas et al., 2005). Scenario 4 correlates to C24n.1n-C22r, with variable low to extremely high sedimentation rates (~10–300 m m.y.$^{-1}$). This scenario is unreasonable due to both the many abrupt changes in sedimentation rate for which there is no lithologic evidence (Fig. 2), and to the extremely high implied sedimentation rates (~300 m m.y.$^{-1}$), which are inconsistent with the observed deposition of lacustrine mudstones and large-scale soil formation.

As a result, scenario 1 is our preferred GPTS placement, which means that the early Eocene climatic optimum is represented in the Salta Basin at Cerro Bayo by fluvial sediments and paleosols within the Maíz Gordo Formation, spanning roughly 53.5–50.5 Ma, based on the linear interpolation through magnetostratigraphic and biostratigraphic tie points (Fig. 2). While recent radioisotopic work from the Green River Basin has recommended possible revisions to this portion of the GPTS (expanding C23n; e.g., Smith et al., 2014; Machlus et al., 2015), these changes do not affect the robustness of the interhemispheric correlation of early Eocene climatic optimum sites, and they have a limited impact on apparent sedimentation rates (~30–40 m m.y.$^{-1}$ vs. 40–50 m m.y.$^{-1}$ for scenario 1). This new age model for the Maíz Gordo Formation thereby allows for a reconstruction of climate conditions in South America that has comparable temporal resolution to other terrestrial sites during the early Eocene climatic optimum interval.

New Climate Results

Ti/Al ratios in these paleosols remained unchanging stratigraphically (μ = 0.05; σ = 0.008; Table DR2 [see footnote 1]) throughout the section at Cerro Bayo, which indicates little or no provenance change through this interval and therefore allows for quantitative reconstructions of paleoclimate (e.g., Sheldon and Tabor, 2009). Using paleosol-based terrestrial climate proxies such as weathering indices of paleosol profiles (CIA-K and SAL of Sheldon et al., 2002; PWI of Gallagher and Sheldon, 2013) and organic carbon isotopic compositions in paleosol A-horizons (e.g., Cotton et al., 2012), the first multiproxy record of terrestrial change during the early Eocene climatic optimum in the temperate Southern Hemisphere has been compiled in Figure 3. The early Eocene climatic optimum is characterized in the Salta Basin by a positive carbon isotope excursion of ~5.7‰ in organic carbon ($\delta^{13}C$), from roughly –26.4‰ to –20.7‰, which occurred around 52 Ma. This carbon isotope change is coupled with an MAT rise of ~3–6 °C, from roughly 9.9 °C to 12.8 °C based on the PWI climofunction, and roughly 6.2 °C to 12.3 °C based on the SAL climofunction (Fig. 3). There is also a consequent MAP increase of ~535 mm yr^{-1}, from roughly 706 mm yr^{-1} to 1242 mm yr^{-1} (Fig. 3). Each excursion recovers to near-baseline values within roughly 1 m.y.

Previous Results

Paleogene terrestrial records from the Northern Hemisphere are known primarily from temperate North America (western United States and Canada), with the most detailed records of the early Eocene climatic optimum derived from basins in Wyoming (Fig. 1; e.g., Greenwood and Wing, 1995; Smith et al., 2008, 2014; Hyland and Sheldon, 2013; Hyland et al., 2013). The early Eocene climatic optimum at these sites is defined by a positive carbon isotope excursion of ~3‰–5‰ in paleosol organic carbon (Fig. 4A) and ~2‰–3‰ in pedogenic carbonates, which corresponds to an ~1000 ppm increase in atmospheric pCO_2 relative to pre– or post–early Eocene climatic optimum concentrations (~500 ppm; Demicco et al., 2003; Hyland and Sheldon, 2013). This greenhouse gas increase was coupled with a temperature rise of ~5–7 °C, indicated by both paleobotanical and paleosol-based proxies (Fig. 4B; Greenwood and Wing, 1995; Hyland and Sheldon, 2013; Hyland et al., 2013), and regional precipitation increases of ~600 mm yr^{-1} (Fig. 4C; Smith et al., 2008; Hyland and Sheldon, 2013; Hyland et al., 2013). Despite difficulties with reproducing global temperature gradients in equable Eocene climates, both regional climate models for North America (e.g., Thrasher and Sloan, 2009) and global climate models (e.g., Shellito et al., 2003; Huber and Caballero, 2011; Lunt

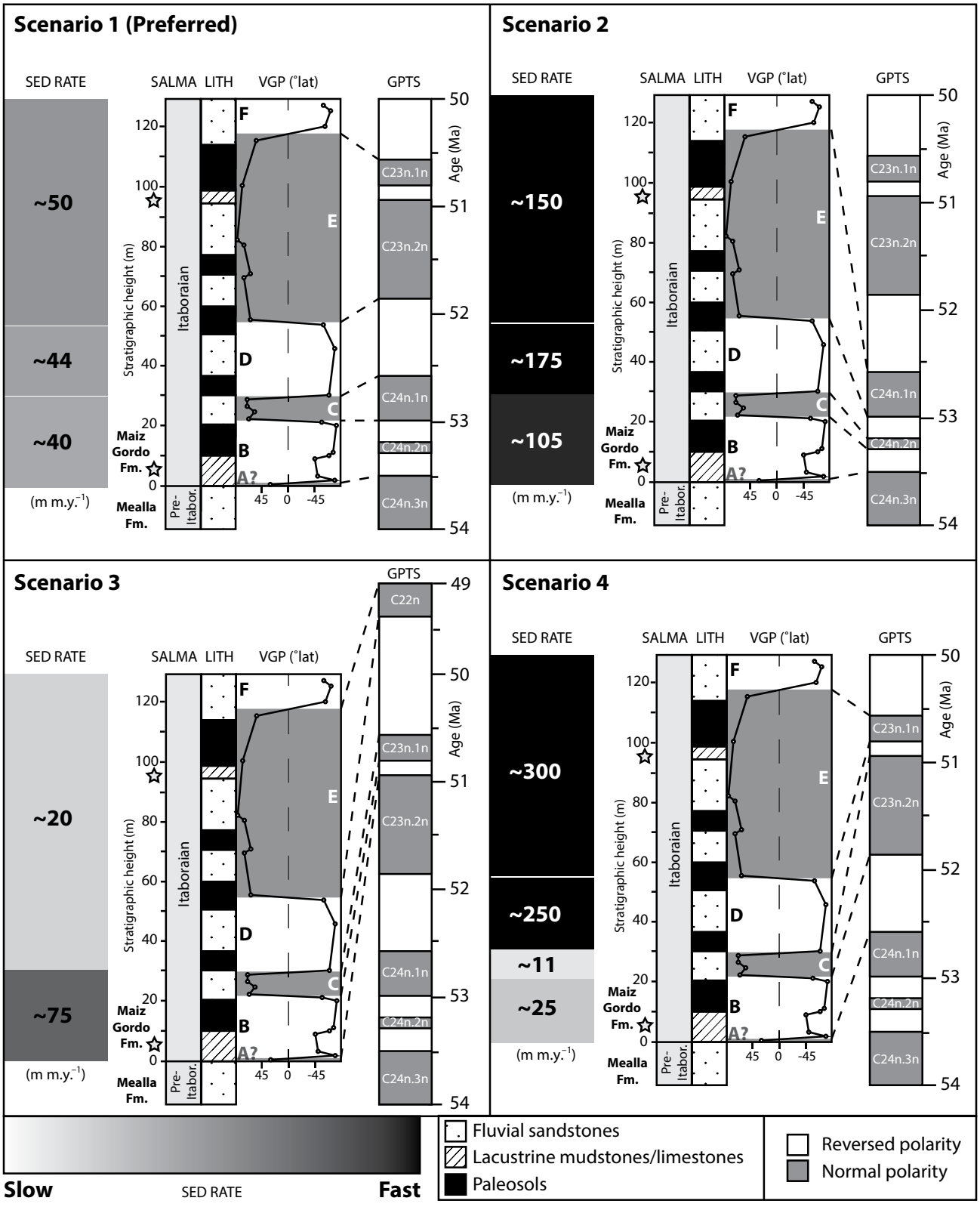

Figure 2. Alternate age model scenarios and potential correlations to the geomagnetic polarity time scale (GPTS; Gradstein et al., 2012), including: (1) preferred correlation to C24n.3n-C22r, with stable moderate sedimentation rates throughout; (2) correlation to C24n.3n-C23r, with stable high sedimentation rates throughout; (3) correlation to C23n.2n-C21r, with variable moderate to low sedimentation rates; and (4) correlation to C24n.1n-C22r, with variable low to extremely high sedimentation rates. SALMA—South American Land Mammal Age; VGP—virtual geomagnetic pole. A–F correspond to local polarity zones.

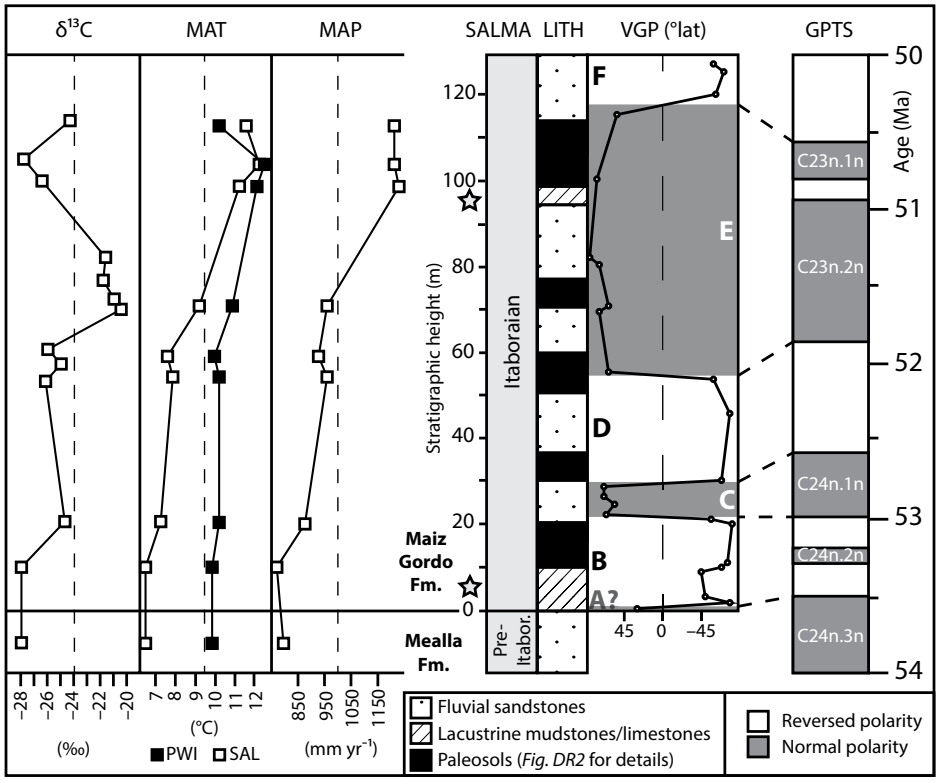

Figure 3. Data from Cerro Bayo. Age interpolation model (preferred scenario from Fig. 2) is based on magnetostratigraphic boundaries (geomagnetic polarity time scale [GPTS]; Gradstein et al., 2012), and sedimentological and paleontological constraints (marker beds starred; Quattrocchio and Volkheimer, 2000; Marquillas et al., 2005; Gelfo et al., 2009), placed within the revised South American Land Mammal Age (SALMA) time scale (Woodburne et al., 2014; Clyde et al., 2014). Climate data from paleosol geochemical proxies include organic carbon stable isotopes ($\delta^{13}C$; standard deviation = 0.27‰), mean annual temperature (MAT) estimates from paleosol weathering index (PWI; standard error = 2 °C) and salinization (SAL; standard error = 4 °C), and mean annual precipitation estimates (MAP; standard error = 182 mm yr^{-1}). VGP—virtual geomagnetic pole. For Figure DR2, see text footnote 1. A–F correspond to local polarity zones.

et al., 2012) suggest that these observed paleoclimatic states as compared with the modern climate at the same latitudes are consistent with elevated atmospheric CO_2 concentrations similar to those predicted via paleobarometry proxy methods (i.e., 2–3× pre–early Eocene climatic optimum).

Previous terrestrial records from the Paleogene of the Southern Hemisphere are more limited, both in terms of carbon isotope records and the limited preservation of paleosols or plant material, though some low-resolution examples exist from basins in Argentina (Fig. 1) that can be expanded as local stratigraphy improves (e.g., Krause et al., 2010). Spatially scattered estimates of paleoclimatic conditions do however identify the early Eocene climatic optimum elsewhere in the Southern Hemisphere, with reconstructed peak MAT ~3–6 °C higher than the Eocene baseline, and peak MAP ~200–600 mm yr^{-1} higher than the Eocene baseline (Fig. 4; Wilf et al., 2003; Retallack, 2008; Krause et al., 2010); however, previous temporal resolution and a lack of paired carbon isotope records had previously been insufficient to evaluate the structure and duration of the peak period.

DISCUSSION

Terrestrial Records

While there is some time-scale uncertainty inherent in such a broad-scale comparison across terrestrial localities in different hemispheres, each of the recently described early Eocene climatic optimum sites (Fig. 1) is fairly well constrained by internal chronologies, and each record has been compiled based on the C23r-C23n boundary, which in each case also corresponds roughly to the initiation of the early Eocene climatic optimum terrestrial carbon isotope excursion (Fig. 4). For purposes of comparison between these records from different hemispheres, with different ranges of absolute values that are reflective of local conditions, we report these data as a magnitude of change (e.g., ΔMAT; Fig. 4) with respect to average values measured before ca. 54 Ma from the same or nearby sites (Fig. 3; Table DR4 [see footnote 1]). For the ΔMAT compilation, we use SAL estimates from Cerro Bayo, as previous methods comparisons suggested that while the PWI climofunction may better estimate absolute temperature in many cases (e.g., Gallagher and Sheldon, 2013), the SAL climofunction most accurately records the magnitude and direction of temperature changes when compared to independent data from isotope and paleobotanical methods (e.g., Hyland and Sheldon, 2013). Based on this overall compilation, terrestrial climate records from the Northern and Southern Hemispheres are in broad agreement in terms of the magnitude and time scale of carbon cycle, temperature, and precipitation changes that occurred at temperate latitudes during the peak early Eocene climatic optimum (Fig. 4).

Paleobotanical records from both hemispheres also indicate variable but significant changes in floral diversity and composition (Wilf et al., 2003; Hyland et al., 2013), which may explain minor differences in the magnitude of the carbon isotope signal observed in different terrestrial localities (Fig. 4A; Smith et al., 2007), given the similarity in climatic conditions between all of the sites. These records of climatic change are remarkably consistent between terrestrial localities, as is the pattern of response showing carbon cycle changes coupled with temperature increases, which are possibly followed by a slight temporal delay before precipitation increases (shaded windows in Fig. 4). The pattern of a slight lag between carbon cycle changes and temperature increases suggests the likelihood of a CO_2 threshold for climate impacts during the early Eocene, possibly linked to a variable or different Earth system response rate or larger buffering capacity for carbon inputs (e.g., Rohling et al., 2012; Jagniecki et al., 2015). The robust link between the temperature and precipitation changes in these records (shaded windows in Fig. 4) is ascribed to the relationship between increased temperatures and higher evaporation/precipitation rates in temperate regions, which is observed in terrestrial records of hyperthermal events like the Paleocene-Eocene thermal maximum (e.g., McInerney and Wing, 2011; Foreman et al., 2012) and is also predicted by modeling experiments of greenhouse conditions (e.g., Held and Soden, 2006).

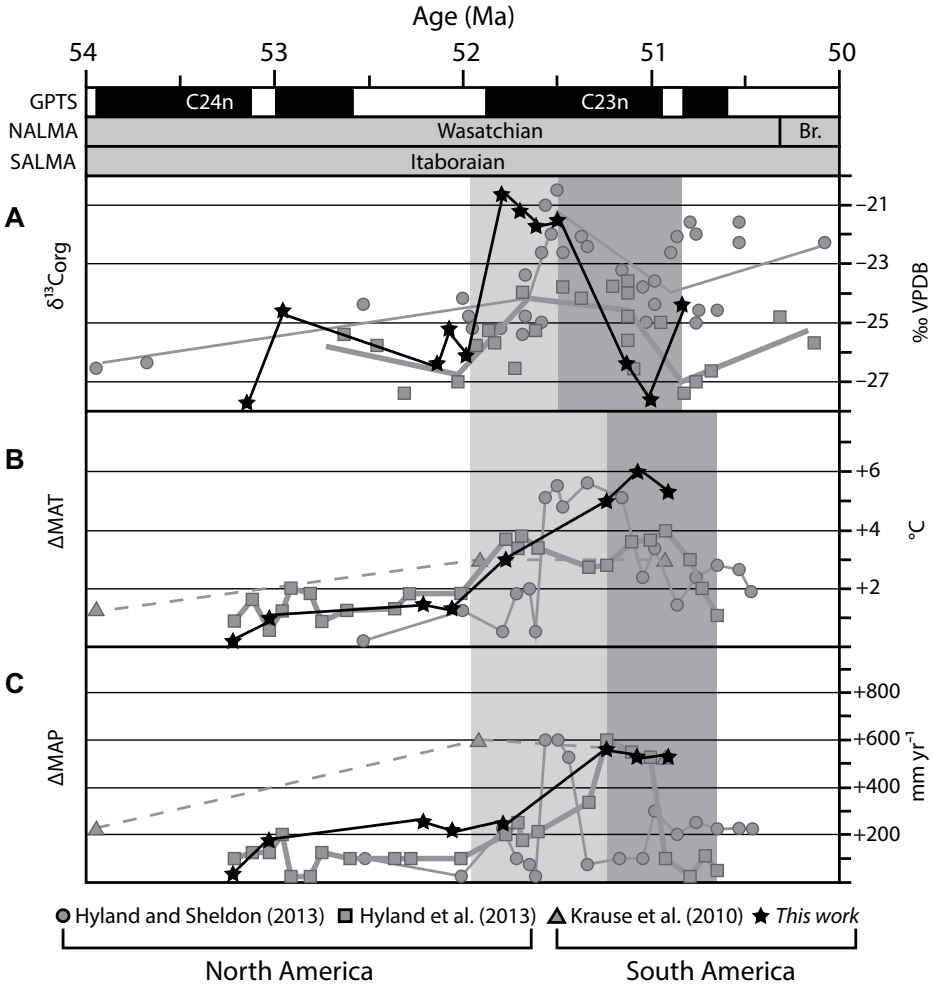

Figure 4. Comparison of (A) carbon isotope ($\delta^{13}C_{org}$), (B) change in mean annual temperature (ΔMAT), and (C) change in mean annual precipitation (ΔMAP) from terrestrial proxy records of the early Eocene climatic optimum at temperate latitudes in both hemispheres. Shaded windows indicate periods of change, with initiation (increasing values; light gray) and recovery (decreasing values, dark gray) phases. GPTS—geomagnetic polarity time scale; NALMA—North American land mammal age; SALMA—South American land mammal age; VPDB—Vienna Peedee belemnite; Br.—Bridgerian.

Terrestrial-Marine Record Comparison

To facilitate a comparison between marine and terrestrial records, data from each have been binned into 250 k.y. bins, averaged, and plotted against one another in Figure 5. While this down-sampling means that processes operating on very short time scales cannot be considered, it provides a means for comparing longer-term changes from records with different amounts of data. Generally speaking, the amount of data per bin is similar (Table DR4 [see footnote 1]), especially when comparing marine and terrestrial ΔMAT values and when comparing marine and terrestrial $\Delta^{13}C$ values. In the context of these records, marine proxy records in both hemispheres also show sizable carbon cycle perturbations during the early Eocene (e.g., Zachos et al., 2008; Hollis et al., 2012), and thus, in a broad sense, both types of records are potentially consistent with increased atmospheric CO_2 concentrations during the early Eocene climatic optimum (e.g., Lunt et al., 2012; Rohling et al., 2012). Similarly, both types of records also show increased temperatures in concert with these carbon cycle changes (Figs. 4 and 5). Terrestrial records indicate slightly enhanced temperature shifts relative to the marine (Fig. 5), which is an unsurprising pattern that has been observed at other major climatic transitions (e.g., Paleocene-Eocene thermal maximum—McInerney and Wing, 2011; Eocene-Oligocene transition—Hren et al., 2013) and previously attributed to the effects of continentality on regional climate responses (isolation and low relative heat capacity of land surfaces as compared with the world's oceans; Rohling et al., 2012).

However, the two types of records diverge in terms of the direction of change of their respective carbon isotope excursions, the timing of the onset of the carbon cycle perturbation (marine before terrestrial), and the time scale over which the resultant systemic shifts are manifest. Terrestrial records of the early Eocene climatic optimum show an average carbon isotope excursion of +5‰ (Fig. 5), whereas marine records show the opposite trend in carbon isotopes, with an average carbon isotope excursion of –1‰ in benthic records and –0.5‰ in planktic records (Fig. 5; e.g., Zachos et al., 2008; Dickens and Backman, 2013). A decoupling between terrestrial and marine carbon isotope excursions, and the difference between planktic and benthic marine excursion magnitudes and timing (Fig. 5) suggest that the carbon cycle conditions of the early Eocene were indeed exceptional (cf., Turner et al., 2014) and point to the transfer of enriched carbon from the deep ocean through the shallow reservoir and into the atmosphere (e.g., Schrag et al., 2013).

In addition to the varied carbon isotope response, the time scales of change are significantly different between the terrestrial record, where climatic changes are characterized by an initiation phase including a variable plateau of peak conditions (~0.5 m.y.) and a subsequent recovery phase (~0.5 m.y.), and the marine record, where the period is characterized by a gradual shift and recovery over a duration of ~2–3 m.y. (Fig. 5; e.g., Zachos et al., 2008; Turner et al., 2014). Furthermore, the terrestrial records also indicate a short (<1 m.y.), intense period of peak warming during an overall period of warmth, whereas the marine records indicate a prolonged warm period without a distinct peak event. These dynamics indicate that the carbon cycle perturbation that led to the peak early Eocene climatic optimum and the following recovery processes operated on an intermediate time scale (0.5–3 m.y.) and affected major carbon pools differently, which makes it possible to use both terrestrial and marine carbon cycle response conditions to differentiate between causal mechanisms in understanding the imbalance between carbon fluxes and burial that resulted in the circumstances of the early Eocene climatic optimum (e.g., Schrag et al., 2013).

Early Eocene Climatic Optimum in the Context of Paleogene Warming

The early Paleogene is defined by long-term (>10 m.y.) warming and includes the apex of Cenozoic warmth during the early Eocene climatic optimum (e.g., Zachos et al., 2008).

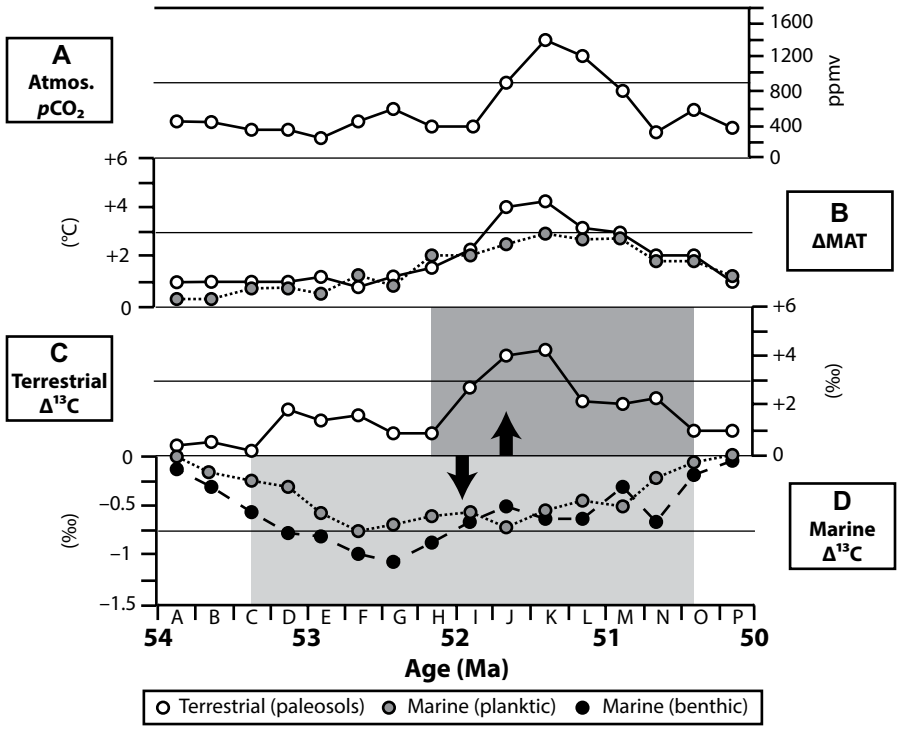

Figure 5. Carbon cycle dynamics during the early Eocene, including: (A) atmospheric carbon dioxide concentrations (modified from Hyland and Sheldon, 2013), (B) terrestrial and marine (Pacific TEX_{86} [tetraether index of 86 carbon atoms] and Mg/Ca; Hollis et al., 2012) temperature excursions (ΔMAT), (C) compiled terrestrial carbon isotope excursions ($\Delta^{13}C$), and (D) marine benthic and planktic carbon isotope excursions (Atlantic, Indian, and Pacific Ocean $\Delta^{13}C$; Zachos et al., 2008; Coccioni et al., 2012; Dickens and Backman, 2013). Displayed points are average values of all data within 250 k.y. windows (A–P) from original sources; actual values are compiled in Table DR4 (see text footnote 1). Arrows highlight the opposite direction of change in isotope records, and shaded boxes indicate distinct time scales of change between marine and terrestrial records.

Numerous short-term hyperthermal events superimposed within the overall warming trend of the Paleogene have been identified and named using marine paleoclimatic records (Cramer et al., 2003; Zachos et al., 2008; Turner et al., 2014). Generally speaking, they represent very short-term (<200 k.y.) climate and carbon cycle fluctuations, and they are normally of relatively modest magnitude, with the obvious exception of the Paleocene-Eocene thermal maximum (McInerney and Wing, 2011). These short-term hyperthermal records also show coherent responses to both carbon cycle and climatic changes between the marine and terrestrial realms (e.g., Paleocene-Eocene thermal maximum—McInerney and Wing, 2011; middle Eocene climatic optimum—Sluijs et al., 2013).

Three of the minor hyperthermal events identified in marine foraminiferal records during this period, the "J," "K," and "L" events (Cramer et al., 2003), occurred within the prolonged early Eocene climatic optimum peak warmth. However, only the "K" event appears to have lasted even 100 k.y. or had a carbon isotope excursion >0.2‰, and in each case, the postevent carbon isotopic values match the pre-event values. In contrast, a "wider-lens" look at the records of the peak early Eocene climatic optimum suggests a moderate-time-scale (≥500 k.y.) change in carbon cycling and climate within this apex of Cenozoic warming, where marine and terrestrial realms exhibited distinct responses (Fig. 5). While it is possible that a series of short-term hyperthermal events remains undiscovered within these longer-term peak warming records and contribute to these differences, the distinct responses likely point instead to a more complex interplay of causal mechanisms during the early Eocene climatic optimum.

Implications for Causal Mechanisms

The contrast in carbon isotope responses has important implications for understanding the global climate system because the interconnections between the marine and terrestrial realms mean that it is unreasonable to consider any of these compiled records separately, which requires that any potential mechanisms of change generate the conditions observed in both systems during the early Eocene climatic optimum. Therefore, the combination of a positive carbon isotope excursion on land and a negative carbon isotope excursion in marine records precludes certain causal mechanisms that would result in a globally negative carbon isotope excursion, such as methane hydrate releases (Dickens, 2003; McInerney and Wing, 2011), orbitally enhanced organic carbon cycles (Turner et al., 2014), or a terrestrial biosphere shift (loss of or change in dominant vegetation type; e.g., Beerling, 2000; Smith et al., 2007). Furthermore, the observed carbon cycle and climate conditions are expressed on an intermediate time scale, suggesting that short-term perturbations (e.g., methane releases, most orbital cycles) may also be insufficient as drivers by themselves.

While longer-term carbon releases from either surface ocean inorganic carbon reservoirs or from enhanced volcanism could result in different carbon isotope excursion patterns both on land and in the oceans, these mechanisms are still inconsistent with proxy records because of the differences in time scale between the observed marine and terrestrial carbon isotope excursions, which are too disparate for stable long-term processes (Schrag et al., 2013). Furthermore, these mechanisms are also incompatible with the substantial atmospheric CO_2 increase recorded by terrestrial proxies, which is likely too large for a typical surface ocean source (Zeebe et al., 2009; Sluijs et al., 2013) or for a volcanic carbon source with an appropriately intermediate duration (e.g., Bryan and Ferrari, 2013).

These conditions point either to: (1) multiple interacting causal mechanisms and carbon cycle–climate feedbacks as yet undescribed for Paleogene climate events, or (2) a potential large-scale carbon transfer to the atmosphere that initiated in the deep marine realm as warming ocean temperatures increased oceanic ventilation and mixing (e.g., Sexton et al., 2011; Green and Huber, 2013; Sluijs et al., 2013). A ventilation/mixing scenario initiating in the deep marine realm could explain the difference in carbon isotope records, driving the removal of isotopically enriched inorganic carbon from the deep ocean reservoir and introducing it into the relatively more depleted atmospheric reservoir, with the surface ocean as an intermediary. As a result, both the surface and larger deep ocean pools would become slightly more depleted in $\delta^{13}C$, producing a minor negative carbon isotope excursion, while the much smaller atmospheric pool would become substantially

more enriched in $\delta^{13}C$, producing a larger positive carbon isotope excursion (e.g., Fig. 5).

Changing ocean ventilation/mixing would also explain the difference in carbon isotope excursion onset timing (marine before terrestrial) and duration of the peak early Eocene climatic optimum in these records (Fig. 5), where carbon cycle changes would have occurred first within ocean reservoirs as ventilation/mixing reorganized oceanic carbon pools, followed by changes in the atmosphere and on land as carbon concentrations in the surface ocean exceeded buffering capacities (e.g., Zeebe, 2012). Subsequent peak atmospheric carbon dioxide concentrations from marine carbon releases could then have been drawn down over time via large-scale carbon burial driven by greenhouse-enhanced marine productivity (e.g., Norris et al., 2013) as well as enhanced continental weathering and marine sedimentation (e.g., Dallanave et al., 2015), which accounts for the observed gradual carbon cycle stabilization and return to baseline Eocene conditions (Fig. 5). While such a scenario is reasonable based on compiled proxy observations, further examination of carbon cycle and ocean circulation dynamics is required through rigorous scenario testing using tools such as: (1) mechanistic carbon cycle models that include both marine and terrestrial conditions and reservoirs (e.g., Zeebe et al., 2009), and (2) paleoplate and paleocean chemistry reconstructions that can identify relevant causal changes in ocean basin geometries and potential circulation patterns (e.g., Norris et al., 2013; van Hinsbergen et al., 2015).

CONCLUSIONS

We present a high-resolution multiproxy record of the early Eocene from the Southern Hemisphere at a site on the margin of the Salta Basin (Argentina), where biostratigraphy and new magnetostratigraphy of the Maíz Gordo Formation indicate that it is early Eocene in age and preserves a sequence of fluvial and paleosol sediments that correspond to the early Eocene climatic optimum. Multiproxy reconstructions from these paleosols record a peak period of carbon isotopic enrichment (up to 5‰ higher), increased MAT (up to 6 °C higher), and increased MAP (up to 500 mm yr^{-1} higher) that is consistent with results compiled from temperate-latitude Northern Hemisphere sites. When paired with marine records of the early Eocene climatic optimum, these consistent aggregated terrestrial responses provide a set of constraints for carbon cycle perturbation scenarios, and, in particular, they highlight substantial differences in time scale and carbon isotope responses between marine and terrestrial records, which could suggest a multiple-mechanism or nontraditional cause for the early Eocene climatic optimum (e.g., changes in ocean ventilation/mixing). This further indicates that paired marine-terrestrial records may be crucial to understanding past changes in the carbon cycle and their impacts on global climate.

ACKNOWLEDGMENTS

We thank J. Guillou and El Servicio Geológico Minero Argentino (SEGEMAR Argentina) for field assistance; R. Van der Voo, M. Dennis, and L. Wingate for laboratory assistance; Z. Guo, G. Dickens, and G. Retallack for comments and discussion during the creation of this manuscript; and the University of Michigan's Rackham Research Grants (to Hyland and Cotton) and ExxonMobil's Geoscience Grants (to Cotton) for funding this research.

REFERENCES CITED

Abels, H.A., Clyde, W.C., Gingerich, P.D., Hilgen, F.J., Fricke, H.C., Bowen, G.J., and Lourens, L.J., 2012, Terrestrial carbon isotope excursions and biotic change during Palaeogene hyperthermals: Nature Geoscience, v. 5, p. 326–329, doi:10.1038/ngeo1427.

Beerling, D.J., 2000, The role of the terrestrial biosphere in Holocene carbon cycle dynamics: Global Ecology and Biogeography, v. 9, p. 421–429, doi:10.1046/j.1365-2699.2000.00202.x.

Bryan, S.E., and Ferrari, L., 2013, Large igneous provinces and silicic large igneous provinces: Progress in our understanding over the last 25 years: Geological Society of America Bulletin, v. 125, p. 1053–1078, doi:10.1130/B30820.1.

Clyde, W.C., Wilf, P., Slingerland, R.L., Barnum, T., Bijl, P.K., Bralower, T.J., Brinkhuis, H., Comer, E.E., Huber, B.T., Ibanez-Mejia, M., Jicha, B.R., Krause, J.M., Schueth, J.D., Singer, B.S., Raigemborn, M.S., Schmitz, M.D., Sluijs, A., and Zamaloa, M., 2014, New age constraints for the Salamanca Formation and lower Rio Chico Group in the western San Jorge Basin, Patagonia, Argentina: Implications for Cretaceous–Paleogene extinction recovery and land mammal age correlations: Geological Society of America Bulletin, v. 126, p. 289–306, doi:10.1130/B30915.1.

Coccioni, R., Bancala, G., Catanzarit, R., Fornaciari, E., Frontalini, F., Giusberti, L., Jovane, L., Luciani, V., Savian, J., and Sprovieri, M., 2012, An integrated stratigraphic record of the Palaeocene–Lower Eocene at Gubbio: New insights into the early Palaeogene hyperthermals and carbon isotope excursions: Terra Nova, v. 24, p. 380–386, doi:10.1111/j.1365-3121.2012.01076.x.

Cotton, J.M., Sheldon, N.D., and Stromberg, C.A.E., 2012, High resolution isotopic record of C_4 photosynthesis of a Miocene grassland: Palaeogeography, Palaeoclimatology, Palaeoecology, v. 337–338, p. 88–98, doi:10.1016/j.palaeo.2012.03.035.

Cramer, B.S., Wright, J.D., Kent, D.V., and Aubry, M.P., 2003, Orbital climate forcing of delta C-13 excursions in the late Paleocene–early Eocene (chrons C24n–C25n): Paleoceanography, v. 18, no. 4, 1097, doi:10.1029/2003PA000909.

Dallanave, E., Agnini, C., Bachtadse, V., Muttoni, G., Crampton, J.S., Strong, C.P., Hines, B.R., Hollis, C.J., and Slotnick, B.S., 2015, Early to middle Eocene magneto-biochronology of the southwest Pacific Ocean and climate influence on sedimentation: Insights from the Mead Stream section, New Zealand: Geological Society of America Bulletin, v. 127, p. 643–660, doi:10.1130/B31147.1.

DeCelles, P.G., Carrapa, B., Horton, B.K., and Gehrels, G.E., 2011, Cenozoic foreland basin system in the Central Andes of northwestern Argentina: Implications for Andean geodynamics and modes of deformation: Tectonics, v. 30, p. 6013–6043, doi:10.1029/2011TC002948.

Demicco, R.V., Lowenstein, T.K., and Hardie, L.A., 2003, Atmospheric pCO_2 since 60 Ma from records of seawater pH, calcium, and primary carbonate mineralogy: Geology, v. 31, p. 793–796, doi:10.1130/G19727.1.

Dickens, G.R., 2003, Rethinking the global carbon cycle with a large, dynamic and microbially mediated gas hydrate capacitor: Earth and Planetary Science Letters, v. 213, p. 169–183, doi:10.1016/S0012-821X(03)00325-X.

Dickens, G.R., and Backman, J., 2013, Core alignment and composite depth scale for the lower Paleogene through uppermost Cretaceous interval at Deep Sea Drilling Project Site 577: Newsletters on Stratigraphy, v. 46, p. 47–68, doi:10.1127/0078-0421/2013/0027.

Driese, S.G., 2004, Pedogenic translocation of Fe in modern and ancient Vertisols and implications for interpretations of the Hekpoort Paleosol (2.25 Ga): The Journal of Geology, v. 112, p. 543–560, doi:10.1086/422665.

Foreman, B.Z., Heller, P.L., and Clementz, M.T., 2012, Fluvial response to abrupt global warming at the Palaeocene/Eocene boundary: Nature, v. 491, p. 92–95, doi:10.1038/nature11513.

Gallagher, T.M, and Sheldon, N.D., 2013, A new paleothermometer for forest paleosols and its implications for Cenozoic climate: Geology, v. 41, p. 647–650.

Gelfo, J.N., Goin, F.J., Woodburne, M.O., and Muizon, C.D., 2009, Biochronological relationships of the earliest South American Paleogene mammalian faunas: Palaeontology, v. 52, p. 251–269, doi:10.1111/j.1475-4983.2008.00835.x.

Gradstein, F.M., Ogg, J.G., Schmitz, M., and Ogg, G., 2012, The Geologic Time Scale 2012: Amsterdam, Netherlands, Elsevier, 1176 p.

Green, J.A.M., and Huber, M., 2013, Tidal dissipation in the early Eocene and implications for ocean mixing: Geophysical Research Letters, v. 40, p. 2707–2713, doi:10.1002/grl.50510.

Greenwood, D.R., and Wing, S.L., 1995, Eocene continental climates and latitudinal temperature gradients: Geology, v. 23, p. 1044–1048, doi:10.1130/0091-7613(1995)023<1044:ECCALT>2.3.CO;2.

Held, I.M., and Soden, B.J., 2006, Robust responses of the hydrological cycle to global warming: Journal of Climate, v. 19, p. 5686–5699, doi:10.1175/JCLI3990.1.

Hollis, C.J., Taylor, K.W.R., Handley, L., Pancost, R.D., Huber, M., Creech, J.B., Hines, B.R., Crouch, E.M., Morgans, H.E.G., Crampton, J.S., Gibbs, S., Pearson, P.N., and Zachos, J.C., 2012, Early Paleogene temperature history of the Southwest Pacific Ocean: Reconciling proxies and models: Earth and Planetary Science Letters, v. 349–350, p. 53–66, doi:10.1016/j.epsl.2012.06.024.

Hren, M., Sheldon, N.D., Bugler, M.J., Grimes, S.T., Hooker, J.J., Collinson, M.E., and Lohmann, K.C., 2013, Terrestrial cooling in northern Europe during the Eocene-Oligocene transition: Proceedings of the National Academy of Sciences of the United States of America, v. 110, p. 7562–7567, doi:10.1073/pnas.1210930110.

Huber, M., and Caballero, R., 2011, The early Eocene equable climate problem revisited: Climate of the Past, v. 7, p. 603–633, doi:10.5194/cp-7-603-2011.

Hyland, E.G., and Sheldon, N.D., 2013, Coupled CO_2-climate response during the early Eocene climatic optimum: Palaeogeography, Palaeoclimatology, Palaeoecology, v. 369, p. 125–135, doi:10.1016/j.palaeo.2012.10.011.

Hyland, E.G., Sheldon, N.D., and Fan, M., 2013, Terrestrial paleoenvironmental reconstructions indicate transient peak warming during the early Eocene climatic optimum: Geological Society of America Bulletin, v. 125, p. 1338–1348, doi:10.1130/B30761.1.

Hyland, E.G., Sheldon, N.D., Van der Voo, R., Badgley, C., and Abrajevitch, A., 2015a, A new paleoprecipitation proxy based on soil magnetic properties: Implications for expanding paleoclimate reconstructions: Geological Society of America Bulletin, v. 127, p. 975–981.

Hyland, E.G., Sheldon, N.D., and Cotton, J.M., 2015b, Terrestrial evidence for a two-stage mid-Paleocene biotic event: Palaeogeography, Palaeoclimatology, Palaeoecology, v. 417, p. 371–378, doi:10.1016/j.palaeo.2014.09.031.

Jagniecki, E.A., Lowenstein, T.K., Jenkins, D.M., and Demicco, R.V., 2015, Eocene atmospheric CO_2 from

the nahcolite proxy: Geology, v. 43, p. 1075–1078, doi:10.1130/G36886.1.

Kent, D.V., and Muttoni, G., 2008, Equatorial convergence of India and early Cenozoic climate trends: Proceedings of the National Academy of Sciences of the United States of America, v. 105, p. 16,065–16,070, doi:10.1073/pnas.0805382105.

Krause, J.M., Bellosi, E.S., and Raigemborn, M.S., 2010, Lateritized tephric palaeosols from central Patagonia, Argentina: A southern high-latitude archive of Palaeogene global greenhouse conditions: Sedimentology, v. 57, p. 1721–1749, doi:10.1111/j.1365-3091.2010.01161.x.

Lunt, D.J., Jones, T.D., Heinemann, M., Huber, M., LeGrande, A., Winguth, A., Loptson, C., Marotzke, J., Roberts, C.D., Tindall, J., Valdes, P., and Winguth, C., 2012, A model-data comparison for a multi-model ensemble of early Eocene atmosphere-ocean simulations: EoMIP: Climate of the Past, v. 8, p. 1717–1736, doi:10.5194/cp-8-1717-2012.

Machlus, M.L., Ramezani, J., Bowring, S., Hemming, S., Tsukui, K., and Clyde, W., 2015, A strategy for cross-calibrating U-Pb chronology and astrochronology of sedimentary sequences: An example from the Green River Formation, Wyoming, USA: Earth and Planetary Science Letters, v. 413, p. 70–78, doi:10.1016/j.epsl.2014.12.009.

Mack, G.H., James, W.C., and Monger, H.C., 1993, Classification of paleosols: Geological Society of America Bulletin, v. 105, p. 129–136, doi:10.1130/0016-7606(1993)105<0129:COP>2.3.CO;2.

Marquillas, R.A., Del Papa, C., and Sabino, I.F., 2005, Sedimentary aspects and paleoenvironmental evolution of a rift basin: Salta Group (Cretaceous–Paleogene), northwestern Argentina: International Journal of Earth Sciences, v. 94, p. 94–113, doi:10.1007/s00531-004-0443-2.

McInerney, F.A., and Wing, S.L., 2011, The Paleocene-Eocene thermal maximum: A perturbation of carbon cycle, climate, and biosphere with implications for the future: Annual Review of Earth and Planetary Sciences, v. 39, p. 489–516, doi:10.1146/annurev-earth-040610-133431.

Natural Resources Conservation Service, 2014, Keys to Soil Taxonomy: Washington, D.C., U.S. Department of Agriculture, 134 p.

Norris, R.D., Turner, S.K., Hull, P.M., and Ridgwell, A., 2013, Marine ecosystem responses to Cenozoic global change: Science, v. 341, p. 492–498, doi:10.1126/science.1240543.

Prezzi, C.B., and Alonso, R.N., 2002, New paleomagnetic data from the northern Argentine Puna: Central Andes rotation pattern reanalyzed: Journal of Geophysical Research–Solid Earth, v. 107, p. 1–18.

Quattrocchio, M.E., and Volkheimer, W., 2000, Paleoclimatic changes during the Paleocene–Lower Eocene in the Salta Group Basin, NW Argentina, *in* Volkheimer, W., and Smelka, A., eds., Southern Hemisphere Paleo- and Neoclimates: Key Sites, Data and Models: New York, Springer, p. 353–367, doi:10.1007/978-3-642-59694-0_22.

Ramón, M.J., and Pueyo, E.L., 2008, Cálculo de direcciones y planos virtuales paleomagnéticas: Ejemplos y comparación con otros métodos: Geotemas, v. 10, p. 1203–1206.

Retallack, G.J., 2001, Soils of the Past: An Introduction to Paleopedology: Boston, Unwin Hyman, 520 p., doi:10.1002/9780470698716.

Retallack, G.J., 2007, Cenozoic paleoclimate on land in North America: The Journal of Geology, v. 115, p. 271–294, doi:10.1086/512753.

Retallack, G.J., 2008, Cool-climate or warm-spike lateritic bauxites at high latitudes?: The Journal of Geology, v. 116, p. 558–570, doi:10.1086/592387.

Rohling, E.J., Sluijs, A., Dijkstra, H.A., and PALAEOSENS Project Members, 2012, Making sense of palaeoclimate sensitivity: Nature, v. 491, p. 683–691, doi:10.1038/nature11574.

Schrag, D.P., Higgins, J.A., Macdonald, F.A., and Johnston, D.T., 2013, Authigenic carbonate and the history of the global carbon cycle: Science, v. 339, p. 540–543, doi:10.1126/science.1229578.

Sexton, P.F., Norris, R.D., Wilson, P.A., Palike, H., Westerhold, T., Rohl, U., Bolton, C.T., and Gibbs, S., 2011, Eocene global warming events driven by ventilation of oceanic dissolved organic carbon: Nature, v. 471, p. 349–352, doi:10.1038/nature09826.

Sheldon, N.D., and Tabor, N.J., 2009, Quantitative paleoenvironmental and paleoclimatic reconstructions using paleosols: Earth-Science Reviews, v. 95, p. 1–52, doi:10.1016/j.earscirev.2009.03.004.

Sheldon, N.D., Retallack, G.J., and Tanaka, S., 2002, Geochemical climofunctions from North American soils and application to paleosols across the Eocene-Oligocene boundary in Oregon: The Journal of Geology, v. 110, p. 687–696, doi:10.1086/342865.

Shellito, C.J., Sloan, L.C., and Huber, M., 2003, Climate model sensitivity to atmospheric CO_2 levels in early-middle Paleogene: Palaeogeography, Palaeoclimatology, Palaeoecology, v. 193, p. 113–123, doi:10.1016/S0031-0182(02)00718-6.

Sluijs, A., Zeebe, R.E., Bijl, P.K., and Bohaty, S.M., 2013, A middle Eocene carbon cycle conundrum: Nature Geoscience, v. 6, p. 429–434, doi:10.1038/ngeo1807.

Smith, F.A., Wing, S.L., and Freeman, K.H., 2007, Magnitude of the carbon isotope excursion at the Paleocene-Eocene thermal maximum: The role of plant community change: Earth and Planetary Science Letters, v. 262, p. 50–65, doi:10.1016/j.epsl.2007.07.021.

Smith, M.E., Carroll, A.R., and Mueller, E.R., 2008, Elevated weathering rates in the Rocky Mountains during the early Eocene climatic optimum: Nature Geoscience, v. 1, p. 370–374, doi:10.1038/ngeo205.

Smith, M.E., Carroll, A.R., Scott, J.J., and Singer, B.S., 2014, Early Eocene carbon isotope excursions and landscape destabilization at eccentricity minima: Green River Formation of Wyoming: Earth and Planetary Science Letters, v. 403, p. 393–406.

Thrasher, B.L., and Sloan, L.C., 2009, Carbon dioxide and the early Eocene climate of western North America: Geology, v. 37, p. 807–810, doi:10.1130/G30090A.1.

Turner, S.K., Sexton, P.F., Charles, C.D., and Norris, R.D., 2014, Persistence of carbon release events through the peak of early Eocene global warmth: Nature Geoscience, v. 7, p. 748–751, doi:10.1038/ngeo2240.

van Hinsbergen, D.J., de Groot, L., van Schaik, S., Spakman, W., Bijl, P., Sluijs, A., Langereis, C., and Brinkhuis, H., 2015, A paleolatitude calculator for paleoclimate studies: PLoS One, v. 10, e0126946-21, doi:10.1371/journal.pone.0126946.

Wilf, P., Cuneo, N.R., Johnson, K.R., Hicks, J.F., Wing, S.L., and Obradovich, J.D., 2003, High plant diversity in Eocene South America: Evidence from Patagonia: Science, v. 300, p. 122–125, doi:10.1126/science.1080475.

Woodburne, M.O., Goin, F.J., Bond, M., Carlini, A.A., Gelfo, J.N., Lopez, G.M., Iglesias, A., and Zimicz, A.N., 2014, Paleogene land mammal faunas of South America: A response to global climatic changes and indigenous floral diversity: Journal of Mammalian Evolution, v. 21, p. 1–73, doi:10.1007/s10914-012-9222-1.

Zachos, J.C., Dickens, G.R., and Zeebe, R.E., 2008, An early Cenozoic perspective on greenhouse warming and carbon-cycle dynamics: Nature, v. 451, p. 279–283, doi:10.1038/nature06588.

Zeebe, R.E., 2012, History of seawater carbonate chemistry, atmospheric CO_2, and ocean acidification: Annual Review of Earth and Planetary Sciences, v. 40, p. 141–165, doi:10.1146/annurev-earth-042711-105521.

Zeebe, R.E., Zachos, J.C., and Dickens, G.R., 2009, Carbon dioxide forcing alone insufficient to explain Palaeocene-Eocene thermal maximum warming: Nature Geoscience, v. 2, p. 576–580, doi:10.1038/ngeo578.

Science Editor: Aaron J. Cavosie
Associate Editor: Xixi Zhao

Manuscript Received 21 January 2016
Revised Manuscript Received 17 July 2016
Manuscript Accepted 20 September 2016

Printed in the USA